Research Square

Preprints are preliminary reports that have not undergone peer review.
They should not be considered conclusive, used to inform clinical practice,
or referenced by the media as validated information.

Protonated Phosphonic Acid Electrodes for High Power Heavy-Duty Vehicle Fuel Cells

Katie Lim
Los Alamos National Laboratory
Albert Lee
Korea Institute of Science and Technology
Vladimir Atanasov
University of Stuttgart
Jochen Kerres
Forschungszentrum Jülich GmbH, Helmholtz Institute Erlangen-Nürnberg for Renewable Energy (IEK-11)
https://orcid.org/0000-0003-4972-6307
Santosh Adhikari
Los Alamos National Laboratory
Sandip Maurya
Los Alamos National Laboratory https://orcid.org/0000-0002-7600-2008
Eun Joo Park
Los Alamos National Laboratory
Luis Delfin
Los Alamos National Laboratory https://orcid.org/0000-0001-5098-1087
Jiyoon Jung
Korea institute of Science and Technology
Fujimoto Cy
Sandia National Laboratory
Ivana Matanovic
University of New Mexico https://orcid.org/0000-0002-9191-8620
Jasna Jankovic
University of Conneticut
Hongfei Jia
Toyota Research Institute of North America https://orcid.org/0000-0003-4515-4807
Yu Seung Kim (yskim@lanl.gov)
Los Alamos National Laboratory https://orcid.org/0000-0002-5446-3890

Article

Keywords: fuel cells, catalysis, vehicle fuel cells

Posted Date: June 7th, 2021

DOI: https://doi.org/10.21203/rs.3.rs-542999/v1

License: This work is licensed under a Creative Commons Attribution 4.0 International License.
Read Full License

Version of Record: A version of this preprint was published at Nature Energy on January 31st, 2022. See the published version at https://doi.org/10.1038/s41560-021-00971-x.

Protonated Phosphonic Acid Electrodes for High Power Heavy-Duty Vehicle Fuel Cells

Katie H. Lim[1⊥], Albert S. Lee[1,2⊥], Vladimir Atanasov[3], Jochen Kerres[3,4,5], Santosh Adhikari[1], Sandip Maurya[1], Eun Joo Park[1], Luis Delfin Manriquez[1], Jiyoon Jung[2], Cy Fujimoto[6], Ivana Matanovic[7], Jasna Jankovic[8], Hongfei Jia[9], and Yu Seung Kim[1*]

[1]MPA-11: Materials Synthesis and Integrated Devices Group, Los Alamos National Laboratory, Los Alamos, New Mexico 87545, USA.

[2]Materials Architecturing Research Center, Korea Institute of Science and Technology, Hwarangno 14gil-5, Seongbuk-gu, Seoul 02792, Republic of Korea.

[3]Institute of Chemical Process Engineering, University of Stuttgart, Boeblinger Str. 78, 70199 Stuttgart, Germany.

[4]Chemical Resource Beneficiation Faculty of Natural Sciences, North-West University, Potchefstroom 2520, South Africa.

[5]Forschungszentrum Jülich GmbH. Helmholtz Institute Erlangen-Nürnberg for Renewable Energies (IEK-11), Egerlandstr. 3, 91058 Erlangen, Germany.

[6]Organic Materials Science, Sandia National Laboratories, Albuquerque, New Mexico 87185, USA.

[7]Department of Chemical and Biological Engineering, Center for Micro-Engineered Materials (CMEM), The University of New Mexico, Albuquerque, New Mexico 87231, USA; Theoretical Division, Los Alamos National Laboratory, Los Alamos, New Mexico 87545, USA.

[8]Materials Science and Engineering Department, University of Connecticut, Storrs, CT 06269, USA.

[9]Toyota Research Institute of North America, Ann Arbor, Michigan 48105, USA.

⊥ These authors contributed equally to this work.

*Correspondence to: yskim@lanl.gov

Fuel cells operating at above 100 °C under anhydrous conditions provide an ideal solution for the heat rejection problem of heavy-duty vehicle applications. Here, we report protonated phosphonic acid electrodes that remarkably improve fuel cell performance. The protonated phosphonic acids are comprised of tetrafluorostyrene phosphonic acid and perfluorosulfonic acid polymers in which a proton of the perfluorosulfonic acid is transferred to the phosphonic acid to enhance the anhydrous proton conduction of fuel cell electrodes. By implementing this material into fuel cell electrodes, we obtained a fuel cell exhibiting a rated power density of 780 milliwatts per square centimeter at 160 °C, with minimal degradation during 2,500 hours of operation, and 700 thermal cycles from 40 to 160 °C under load.

Hydrogen fuel cells are attractive devices for automotive applications with benefits such as: extended driving range, swift refueling time of internal combustion engine vehicles, and environmental benefits[1]. While the commercialization of clean, high-efficiency fuel cell electric vehicles has been successfully launched, further technological innovations are needed for the next generation fuel cell platform to evolve for heavy-duty vehicles (HDVs) including trucks and buses, as well as marine, rail, and aviation applications[2-4]. One of the most significant technical challenges of HDV fuel cells is the issue of heat rejection as the average operating temperature of HDV fuel cells can be 5 – 15 °C higher than light-duty vehicle fuel cells[5]. There is an easy solution for heat rejection in diesel engines since much of the engine heat waste at high temperatures (250 °C at idle and up to 700 °C at full load) is simply removed by high temperature gases leaving the tail pipe. In current low-temperature polymer electrolyte membrane fuel cells (LT-PEMFCs), the heat rejection requirement is met by operating the fuel cell at a high cell voltage, ca. 0.76 V at 80 °C[6], in which the power generated is < 0.45 W cm^{-2}. To achieve an efficient fuel cell powered engine on par with a diesel engine, the operating temperature of fuel cell stacks must increase to the engine coolant temperature (100 °C) and ideally up to 160 °C so that the high power can be obtained at a reduced cell voltage (0.43 V). The high-temperature operation of fuel cells has further advantages. The cost of fuel cell systems can be reduced by downsizing the fuel cell cooling system, providing flexibility of aerodynamic vehicle design. Additionally, high-temperature and dry operation allows for the use of reformate hydrogen containing 2% carbon monoxide[7] and enables operation of the system without a large humidifier or complex temperature/humidity controller unit[8]. However, increasing operating temperature for LT-PEMFCs also has overwhelming challenges because perfluorosulfonic acid (PFSA) electrolytes require adequate hydration which is difficult when the cell operates at > 100 °C due to high water partial vapor pressure[9]. Therefore, extensive research efforts to develop polymer electrolytes for high-temperature polymer electrolyte membrane fuel cells (HT-PEMFCs) have been undertaken over the last decade.

The most popular HT-PEMFCs use a phosphoric acid-doped polybenzimidazole (PA-PBI)[10,11]. However, PA-PBI HT-PEMFCs have been considered only for stationary applications because these cells are difficult to operate below 140 °C without suffering from the loss of phosphoric acid. For automotive fuel cells, a wide range of operating temperatures (80 – 200 °C) is desirable for dynamic operation and reduction of the battery size for fuel cell start-up. Furthermore, limited durability of PA-PBI HT-PEMFCs during start up-shutdown[12] and normal vehicle drive cycles make it unsuitable for automotive applications. We reported that HT-PEMFCs based on a quaternary ammonium-biphosphate ion-pair coordination (ion-pair HT-PEMFCs) exhibited excellent phosphoric acid retention at 80 – 160 °C [13] by shifting the phosphoric acid partition composition through much stronger ionic interactions[14]. However, the performance of ion-pair HT-PEMFCs was poor because of electrode flooding by the high concentration of phosphoric acid in the ion-pair ionomer-bonded cathode. Phosphonated polymers are a potential candidate as the electrode binder as they do not have a liquid acid component. Early attempts to use phosphonated polymers in fuel cell electrodes were unsuccessful because the formation of a phosphonic acid anhydride which limited the anhydrous proton conductivity at > 100 °C[15,16]. Recently, we resolved this issue by implementing a highly electron-withdrawing fluorophenyl substituent that suppresses the undesirable phosphonic acid anhydride formation[17]. Improved fuel cell performance was obtained by a poly(2,3,5,6-tetrafluorostyrene-4-phosphonic acid) (PWN) ionomer. However, further performance improvement is required for the ion-pair HT-PEMFCs to be commercially viable for HDV applications as the ion-pair HT-PEMFCs achieved only marginal rated power improvement compared to state-of-the art LT-PEMFCs (**Table 1**).

Table 1. Comparison of the H_2/air performance of current polymer electrolyte fuel cells

PEM (thickness)	PEM component		Electrode binder	Cathode catalyst ($mg_{Pt}cm^{-2}$)	Operating conditions		Power density [a] ($W\ cm^{-2}$)			Ref.
	Coordination	Medium			Temp. (°C)	RH (%)	@0.7 V	Rated	Peak	
Nafion (≤25 μm)	SO_3^-(anion) + H_3O^+(cation)	H_2O	Nafion	PtCo (0.1)	80 ± 15	> 30	0.84	0.32	> 1	(*18*)
PA-PBI (40 μm)	$C_7H_6N_2$(base) + H_3PO_4(acid)	H_3PO_4	PTFE	Pt/C (0.83)	160 ± 20	0	0.07	0.43	0.43	(*19*)
Ion-pair (120 μm)	NR_4^+(cation) + $H_2PO_4^-$(anion)	H_3PO_4	Ion-pair	Pt/C (0.6)	160 ± 60	0	0.05	0.28	0.30	(*13*)
Ion-pair (40 μm)			Phosphona-ted	Pt/C (0.6)			0.12	0.48	0.48	(17)

[a] H_2/air performance measured at 80 °C for LT-PEMFC and 160 °C for PA-PBI and ion-pair HT-PEMFCs.

Here, we report on the protonation of phosphonic acids that increase proton conductivity more than an order of magnitude compared to the previous non-protonated PWN ionomer. We show the experimental and theoretical evidence on the protonation of phosphonic acids which is distinctive from the hydrogen-bonding interaction of phosphonic acids. Based on this concept, we designed protonated phosphonic acid electrodes that enable remarkable rated power density and are thus suitable for HDV fuel cells.

Protonated phosphonic acid ionomer for ion-pair HT-PEMFCs

To increase the performance of ion-pair HT-PEMFCs, we consider protonation of phosphonic acid by transferring a proton from perfluorosulfonic acid (PFSA) that has stronger acidic moiety (**Fig. 1A**). For example, the pK_a of pentafluorophenylphosphonic acid (PFPA) decreases from 1.3 to -0.4 when a proton from PFSA (pK_a = -14) is transferred to the phosphonic acid (**Fig. S1A**). The density functional theory (DFT) calculations indicate that the proton transfer from fluoroethanesulfonic acid to PFPA is a spontaneous process ($\Delta_r G$ = -4.7 kJ mol^{-1}) with a small kinetic barrier of 5.0 kJ mol^{-1} (**Fig. 1B**). To probe the protonation of phosphonic acid, we prepared a composite ionomer by blending PWN and Nafion (**Fig. 1C**). The nature of interactions of the composite ionomer was investigated by ^{31}P NMR (**Fig. 1D**). As the composition of Nafion increased, the phosphorus peak broadened and four distinctive peaks evolved. Similarly, ^{31}P NMR signal splitting was observed with gallium orthophosphate solutions[20]. The assignment of the ^{31}P NMR peaks was made based on the calculation of the change in the ^{31}P NMR chemical shift of PFPA when PFPA was coordinated with fluoroethanesulfonic acid (**Fig. S1B**). The DFT calculations show that the ^{31}P NMR signal of PWN exhibits an upfield shift of 1.9 ppm when PWN is coordinated with one sulfonic acid equivalent of Nafion. In this case, the coordination is realized via a phosphonic oxygen of PWN and SO_3H group of Nafion. When additional hydrogen bonds form between the phosphonic POH groups of PWN and sulfonic oxygen atoms in sulfonic acid of Nafion, the ^{31}P NMR signal of PWN shifts downfield to +1.6 and +2.2 ppm (peaks P3 and P4). Note that the DFT calculation also shows that one sulfonic acid group can interact with multiple phosphonic acids as the sulfonic acid group has multiple coordination sites. First-principles calculations using the MP2/6-31 G(d) level of theory[21] further show that the anhydride formation of the protonated PFPA is 13.5 kcal mol^{-1} more endergonic than that of the non-protonated PFPA at 160 °C (**Fig. 1E**). The higher Gibbs free energy for anhydride formation of the protonated PFPA may be attributed to the smaller pK_a which makes protonation of this acid energetically more difficult as shown in the linear correlation between pK_a of various phosphonic acids[22] and the Gibbs free energy for acid anhydride formation (**Fig. 1F**).

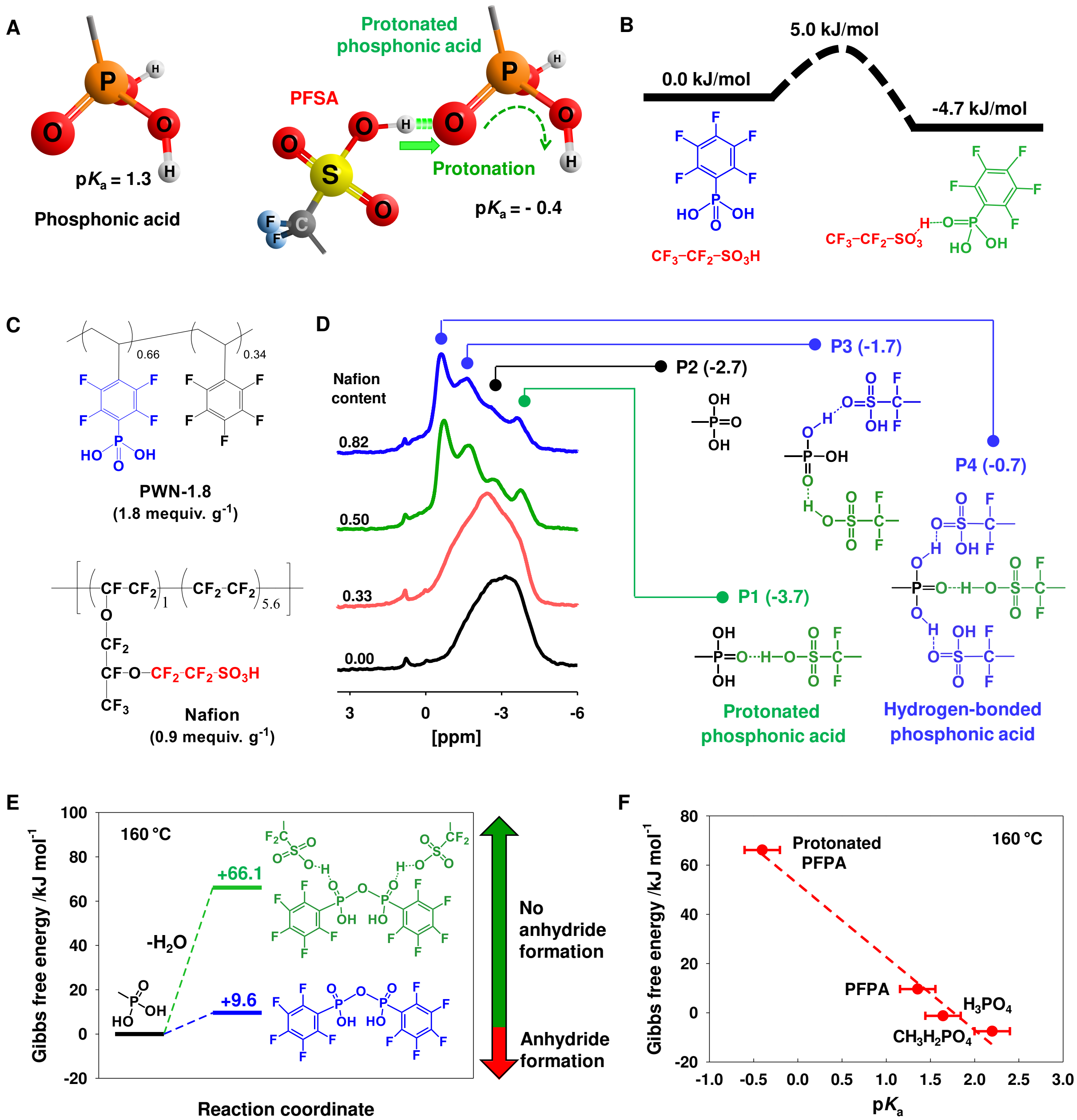

Figure 1 | Protonation of phosphonic acid. (A) Schematic illustration of protonation of phosphonic acid and the pK_a value change of PFPA after protonation. **(B)** Energetics of proton transfer for PFPA from PFSA (DFT results). **(C)** Chemical structures and ion exchange capacity (IEC, mequiv. g^{-1}) of PWN-1.8 and Nafion. **(D)** ^{31}P NMR of Nafion/PWN mixture in dimethyl sulfoxide-*d*6 (DMSO-d_6) as a function of Nafion content. **(E)** Gibbs free energy diagrams for the anhydride formation at 160 °C: protonated PFPA (green) and non-protonated PFPA (blue). **(F)** Correlation between the pK_a values of various phosphonic acids and the Gibbs free energy of phosphonic acid anhydride formation. The error bar of ± 0.2 pK_a units was determined as a root-mean-square error in the fit of the experimental pK_a values to the DFT-calculated difference in the electronic energy of protonated and deprotonated forms of an acid.

Proton conductivity study on protonated phosphonic acid

The increased acidity of protonated PFPA not only prevents undesirable phosphonic acid anhydride formation but also increases proton conductivity. **Fig. 2A** shows the proton conductivity of the PWN and Nafion/PWN composite in anhydrous *N*-methyl-2-pyrrolidone (NMP) dispersion measured as a function of IEC of PWN. The conductivity of the Nafion (dark grey bar) was 2.0 mS cm^{-1}. The conductivity of the PWN (green bar) increased from 0.2 to 2.9 mS cm^{-1} as the IEC of the phosphonated polymers increased from 0 to 3.0 mequiv. g^{-1}. The non-zero proton conductivity of PWN-0 is probably due to residual water, ca. 0.1 % in the system. As the IEC of the PWN increased from 1.3 to 1.8 mequiv. g^{-1}, the proton conductivity significantly increased which suggests that the concentration of the protons in the dispersion is high enough at the IEC to pass the percolation threshold and form statistically more channels that can transport protons. The proton conductivity of the composite polymers (purple bar) was lower than the average value of the individual Nafion and PWN (orange bar), when the IEC of the PWN was below 1.5 mequiv. g^{-1}, but the composites' proton conductivity exceeded the average value of the individual components when the IEC of PWN was > 1.5 mequiv. g^{-1}. This result shows that adding PFSA to PWN with a low IEC does not increase proton conductivity although adding PFSA to PWN with a high IEC effectively increases proton conductivity. The same behavior was observed in the dispersion conductivity using DMSO (**Fig. S3**). This result suggests that only the protonated phosphonic acid that corresponds to P1 of ^{31}P NMR contributes to increased proton conductivity while the hydrogen-bonded phosphonic acid that corresponds to P2 and P3 in ^{31}P NMR plays a minor role in enhancing conductivity. This is because the P1 interaction (P=O··H-O-S) enhances the acidity of the phosphonic acid, while P2 and P3 interactions (P-O-H··O=S) limit the proton mobility of the phosphonic acid by hydrogen-bonding interaction. The impact of IEC on the PWN of the Nafion/PWN composite ionomers on fuel cell performance was examined under H_2/O_2 conditions (**Fig. 2B**). High-angle annular dark field (HAADF)-scanning transmission electron microscope (STEM) images and corresponding energy-dispersive X-ray (EDS) elemental maps (Pt + F+ C) of the gas diffusion electrodes indicated that the composite ionomers are uniformly distributed within the electrodes with preferential ionomer distribution to the catalyst nanoparticles (**Fig. S2**). The MEA employing the Nafion/PWN-1.8 and 3.0 composite ionomers outperformed the MEAs using the

Nafion/PWN-0.9 ionomer that have a greater number of hydrogen-bonded phosphonic acids. Electrochemical impedance spectroscopy (EIS) analysis indicated that the charge transfer and mass transport resistance of the Nafion/PWN-0.9 ionomer-bonded electrodes substantially increased as the cell voltage decreased (**Fig. S4**). This result suggests that the Nafion/PWN-0.9 inhibits mass transport as well as proton conduction.

We investigated the impact of the Nafion content on proton conductivity using a Nafion/PWN-1.8 composite ionomer. The proton conductivity of the composites increased as the content of the PWN increased, but deviated from the average value (blue dash line), which confirms the enhancement of proton conductivity by protonation (**Fig. 2C**). Note that the most significant conductivity deviation was observed at a Nafion content of ca. 0.35 where the highest degree of protonated phosphonic acid is formed with P=O··H-O-S interactions (P1) as shown in ^{31}P NMR in **Fig. 1D**. When compared with the conductivity of the non-protonated PWN (gray dash line), the conductivity of the Nafion/PWN-1.8 composites was significantly higher. For example, at an IEC of 0.9 mequiv. g^{-1}, the conductivity of the protonated phosphonic acid is 0.9 mS cm^{-1}, ~50% higher than that of the non-protonated phosphonic acid (0.6 mS cm^{-1}). The fuel cell performance using Nafion, non-protonated phosphonic acid, and protonated phosphonated (Nafion content = 0.4) ionomers was evaluated at 160 °C under H_2/O_2 conditions (**Fig. 2D**). A significant performance improvement was observed when the electrode binder was changed from Nafion to the non-protonated and protonated phosphonic acid ionomers. The peak power density (PPD) were 0.96, 1.30 and 1.67 W cm^{-2} for the Nafion, non-protonated, and protonated phosphonic acid ionomer-bonded MEAs, respectively. The lower charge transfer resistance of the protonated ionomer-bonded electrode at 0.8 V (0.7 vs. 1.0 Ω cm^2 for non-protonated electrode) confirms that the higher proton conductivity of the protonated phosphonic acid enhances electrode kinetic performance (**Fig. S5**). The Nafion-bonded MEA has much higher ohmic and mass transport resistance at 2.0 A cm^{-2}. Between the four protonated phosphonated ionomers, the ionomer with the Nafion contents of 0.3 and 0.4 exhibited the best performance (**Fig. S6**) consistent with the Nafion to PWN ratio that showed the most pronounced effect of protonation shown in the ^{31}P NMR and the dispersion conductivity measurements (**Figures 1D** and **2C**).

We investigate the proton conductivity of the dispersion-cast membranes cast from DMSO dispersion (details in the supplementary information; and **Fig. S7**). The conductivity of phosphonated membranes is known to be sensitive to humidification and phosphonic acid concentration, i.e., IEC. For example, the proton conductivity PWN-1.8 exposed at 35% RH at room temperature is 0.06 mS cm^{-1} at 80 °C, while the anhydrous conductivity of the same polymer is only 5×10^{-4} mS cm^{-1} at the same temperature[17]. Because water is generated in the cathode and phosphoric acid movement and redistribution under fuel cell operating conditions[23], the ionomer conductivity in the fuel cell electrodes is better estimated with a phosphoric acid-doped ionomer. **Fig. 2E** shows that the proton conductivity of the protonated PWN (phosphoric acid-doped) membrane was more than an order of magnitude higher than the non-protonated phosphonic acid (phosphoric acid-doped) membrane. For example, the proton conductivity of the protonated PWN was 7.0 mS cm^{-1} at 160 °C, while the proton conductivity of the non-protonated PWN was only 0.2 mS cm^{-1}. The un-doped PWN exhibited much lower conductivity (0.01 mS cm^{-1} at 160 °C) than the phosphoric acid-doped PWN, suggesting that phosphoric acid redistribution plays a significant role in electrode performance that explains the synergistic effect of the use of phosphonated ionomers with ion-pair membranes. **Fig. 2F** shows the operating temperature effect on fuel cell performance of an MEA employing the Nafion/PWN-1.8 ionomer. As expected, the fuel cell performance increased with operating temperature with the PPD of the MEA increasing from 0.53 to 2.01 W cm^{-2} as the operating temperature increased from 80 to 200 °C. The change of the high frequency resistance (HFR) of the cell between 80 and 200 °C is relatively small (e.g., 0.064 Ω cm^2 for 80 °C vs. 0.045 Ω cm^2 for 200 °C at 2 A cm^{-2}) (**Fig. S8**) primarily because the proton conductivity of the ion-pair membrane has little dependence on temperature[13]. This result suggests that the significant performance improvement with temperature is mostly attributed to electrode performance. Considering the PPDs of a recent SnP_2O_7-based intermediate temperature fuel cell[24] and a non-protonated phosphonic acid ionomer-doped HT-PEMFC[17] at 200 °C which are 0.71 and 1.50 W cm^{-2}, respectively, the performance improvement shown with the protonated phosphonated ionomer-bonded MEA is remarkable.

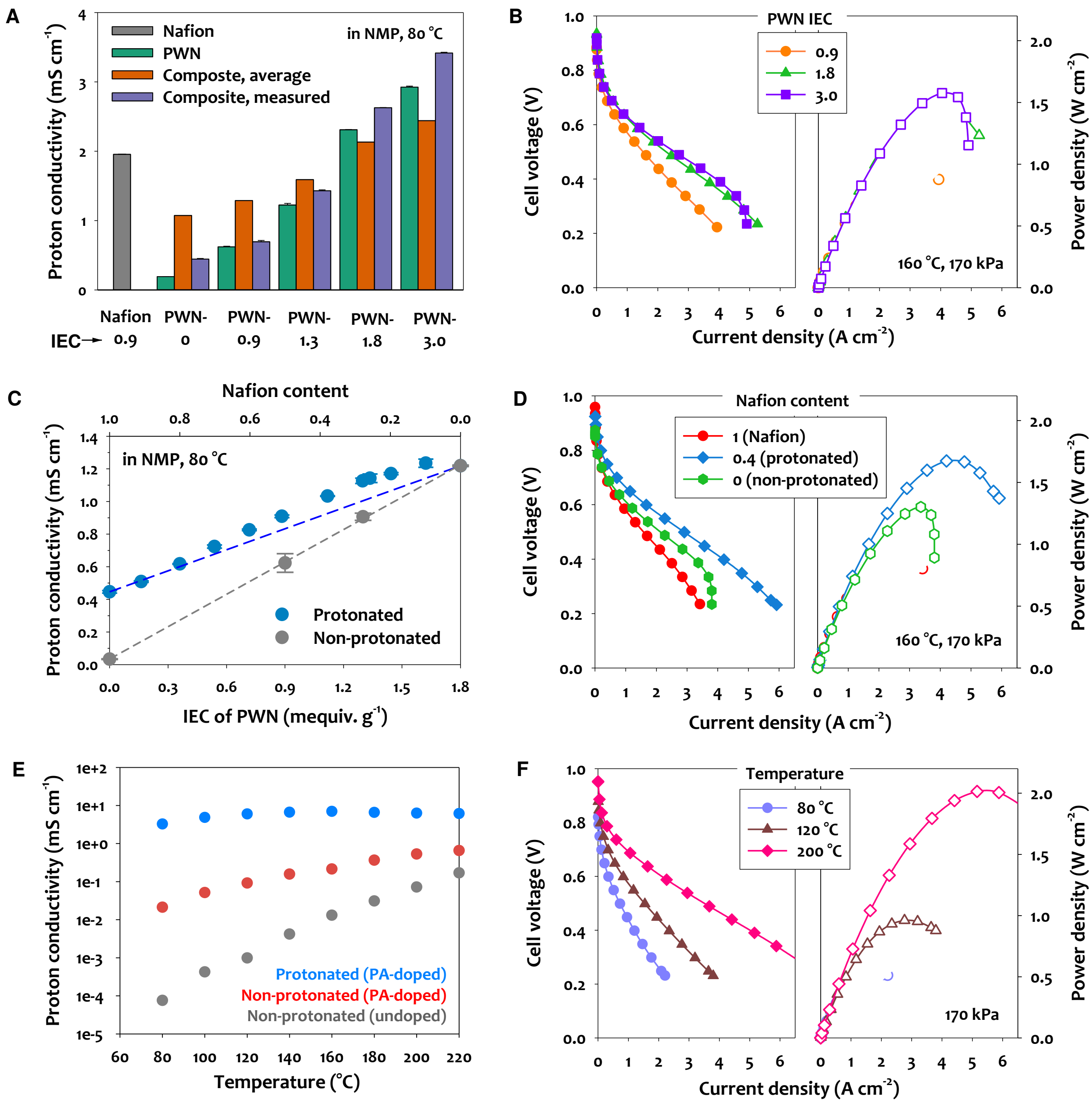

Figure 2 | Impact of protonation on proton conductivity and fuel cell performance. (A) Proton conductivity of Nafion, PWN, and Nafion/PWN mixture in NMP (solid content: 5 wt%). The Nafion content (weight ratio) of the composite ionomers = 0.5. **(B)** H_2/O_2 fuel cell performance of MEAs employing Nafion/PWN composite ionomers as a function of IEC of PWN (Nafion content = 0.5). The MEA components: biphosphate quaternary ammonium ion-pair (QAPOH-PA) membrane (35 μm thickness), anode (Pt-Ru/C, 0.5 mg_{Pt} cm^{-2}) and cathode (Pt/C, 0.7 mg_{Pt} cm^{-2}). **(C)** Proton conductivity of Nafion/PWN-1.8 in NMP (solid content: 2.5 wt%) as a function of Nafion content. **(D)** H_2/O_2 fuel cell performance of MEAs employing Nafion/PWN-1.8 as a function of Nafion content. The MEA components: biphosphate quaternary ammonium ion-pair (QAPOH-PA) membrane (35 μm thickness), anode (Pt-Ru/C, 0.5 mg_{Pt} cm^{-2}) and cathode (Pt/C, 0.7 mg_{Pt} cm^{-2}). **(E)** Anhydrous proton conductivity comparison of protonated (Nafion/PWN-1.8, Nafion content: 0.4) and non-protonated PWN (PWN-1.1) membranes after phosphoric acid doping as a function of temperature. The concentration of phosphonic acids in both membranes is the same (1.1 mequiv. g^{-1}) for fair comparison. Proton conductivity of non-protonated PWN membrane (IEC = 1.8 mequiv. g^{-1})[17] was used for comparison purpose. **(F)** H_2/O_2 fuel cell performance of MEAs employing Nafion/PWN-1.8 (Nafion content = 0.4) as a function of temperature. The MEA components: biphosphate quaternary ammonium ion-pair (QAPOH-PA) membrane (35 μm thickness), anode (Pt-Ru/C, 0.5 mg_{Pt} cm^{-2}) and cathode (Pt/C, 0.7 mg_{Pt} cm^{-2}).

Fuel cell performance comparison

We compare the performance of the ion-pair HT-PEMFC using a protonated phosphonic acid ionomer (Nafion/PWN-1.8) with a commercial PA-PBI HT-PEMFC, LT-PEMFC, and anion exchange membrane fuel cell (AEMFC) under H_2/air conditions. The rated power density of these three fuel cell systems was calculated at their optimum operating temperatures (See materials and methods for the calculation details). The commercial PA-PBI HT-PEMFC showed a rated power density of 0.50 W cm^{-2} with a HFR of 0.064 Ω cm^2 at 0.43 V and 160 °C (**Fig. 3A**). The rated peak power density of the ion-pair HT-PEMFC was 0.78 W cm^{-2} with a HFR of 0.048 Ω cm^2 at 160 °C. The kinetic performance of the ion-pair HT-PEMFC was higher than that of the PA-PBI HT-PEMFC at high cell voltages although the difference is less significant. The rated power density of a commercial LT-PEMFC was 0.41 W cm^{-2} with a HFR of 0.043 Ω cm^2 at 0.76 V and 80 °C under fully hydrated conditions (**Fig. 3B**). The rated power density of the LT-PEMFC at 80 °C was ~53% of the ion-pair HT-PEMFC at 160 °C. The rated power density of the LT-PEMFC at 100 °C increased to 0.78 W cm^{-2} at 100% inlet RH but decreased to 0.29 W cm^{-2} at 40% inlet RH (**Fig. S9**). Besides the rated power, the current density of the ion-pair HT-PEMFC reached 2.7 A cm^{-2} under anhydrous conditions may have a cost benefit over the LT-PEMFC that need complicated and expensive bipolar plates and a microporous layer for the lower current density under fully hydrated conditions. The AEMFC using a quaternary ammonium functionalized poly(phenylene) membrane showed a similar rated power with a higher HFR (0.62 Ω cm^2) at 80 °C under fully hydrated conditions[25]. The kinetic performance of the LT-PEMFC and AEMFC is substantially higher than that of the ion-pair HT-PEMFC, e.g., ~ 0.6 vs 0.2 W cm^{-2} (ion-pair HT-PEMFC) at 0.7 V suggesting a remaining task of further improving catalysts of the ion-pair HT-PEMFC.

We also compare the effect of cathode Pt loading on the ion-pair HT-PEMFC performance (**Fig. S10**). We used three different commercial Pt/C catalysts (Pt on high surface area carbon) for this study, i.e., HiSPEC 9100 (Pt 60%), TEC10E40E (Pt 40%) and TEC10E20E (Pt 20%). At a given catalyst loading, the Pt/C catalyst with a higher Pt content showed higher performance. For the HiSPEC 9100 and TEC10E40E, the MEA with 0.3 mg cm^{-2} cathode Pt loading exhibited comparable performance to the MEAs with 0.6 mg cm^{-2} cathode Pt loading. The MEAs with 0.1 mg cm^{-2} cathode Pt loading showed notable performance loss. The TEC10E10E (Pt 20%) catalyzed MEA showed more significant performance loss as the cathode loading decreased to 0.1 mg cm^{-2}. This result suggests that the use of a Pt catalyst with a high Pt to carbon ratio is beneficial to the protonated ionomer-bonded cathode. The effect of the reactant gas flow rate on performance was also investigated (**Fig. S11**). As expected, the fuel cell performance increased as the gas flow rate increased from 500 to 2,000 standard cubic centimeters per minute (sccm). With 2,000 sccm, the peak power density of the ion-pair HT-PEMFC reached to 1 W cm^{-2} at 160 °C.

Fig. 3C portrays the paradigm shift that emerges from the experiments involving ion-pair HT-PEMFCs. The rated power density of state-of-the-art LT-PEMFCs using advanced catalysts (blue bars)[18,26,27] is ~0.4 W cm^{-2} at 80 °C. When compared to the state-of-the-art LT-PEMFC, the rated power of the ion-pair HT-PEMFC (purple bar) at 160 °C is approximately two times higher. While the rated power density of the LT-PEMFCs could be increased to ~1.0 W cm^{-2} at 95 °C, the durability of LT-PEMFCs at the operating temperature is a concern[28]. The rated power of ion-pair HT-PEMFCs also increased with temperature and could achieve the LT-PEMFC benchmark performance at ~200 °C. AEMFCs (green bar) have a similar rated power density to LT-PEMFCs at 80 °C yet with high Pt loading[25,29,30]. The PA-PBI HT-PEMFCs (red bars) have a rated power density of 0.42 – 0.53 W cm^{-2} at 160 °C[19,31-33]. However, the rated power density did not increase at 200 °C due to possible evaporation of phosphoric acid. At the intermediate temperature (120 °C), all fuel cells suffered from relatively low performance. Nevertheless, the ion-pair HT-PEMFC exhibited the highest performance (PPD = 0.48 W cm^{-2} vs. 0.39 W cm^{-2} for PA-PBI HT-PEMFC and 0.35 W cm^{-2} for the LT-PEMFC at 80% inlet RH) (**Fig. S12**).

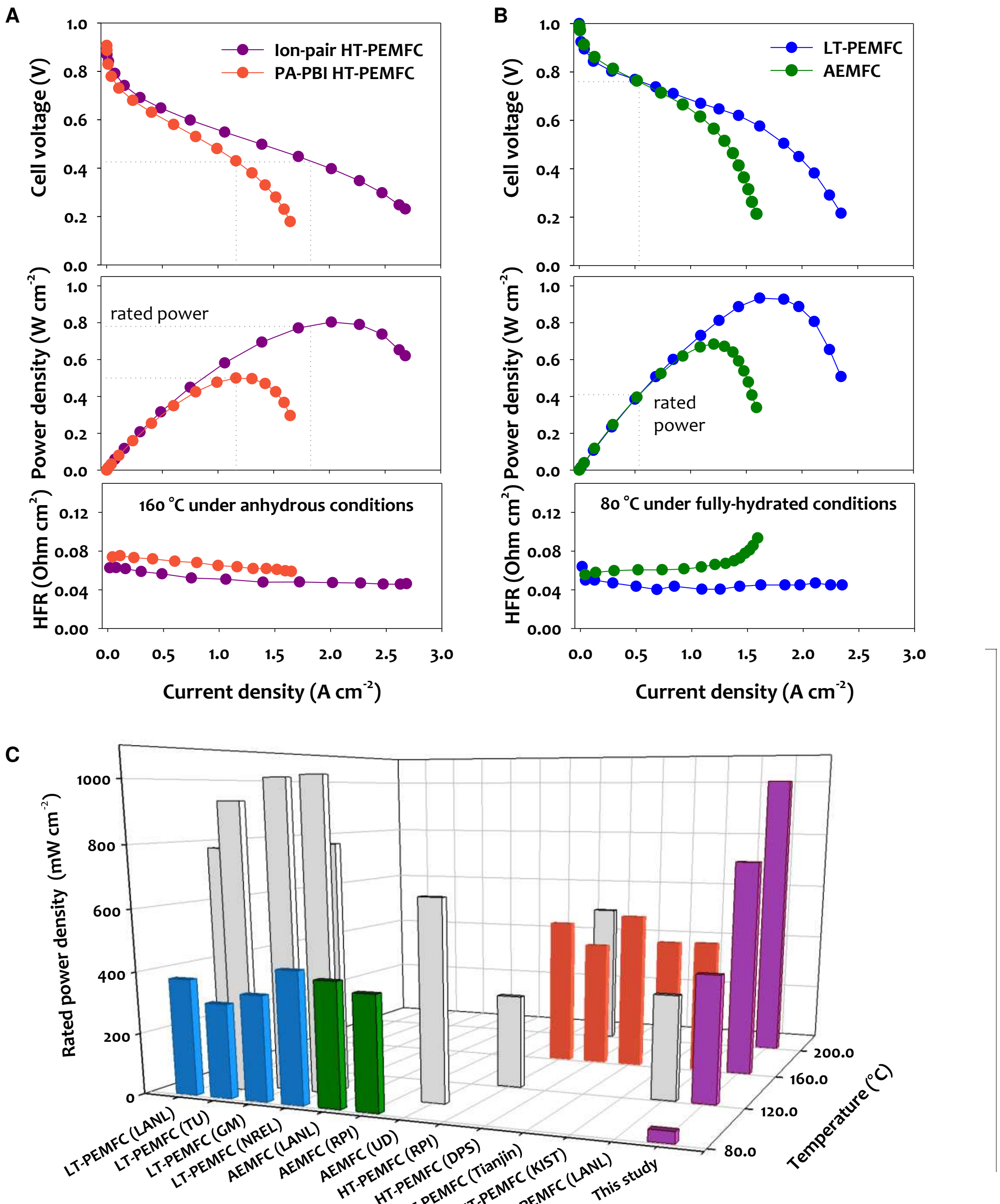

Figure 3 | H_2/air fuel cell performance comparison. (A) *i*-*V* curve and power density of ion-pair and PA-PBI HT-PEMFCs at 160 °C, 148 kPa (abs) backpressure and H_2/air flows (500/500 sccm) under anhydrous conditions. Protonated ionomer-bonded MEA component: QAPOH-PA membrane (35 μm thickness), Nafion/ PWN-1.8 ionomer (Nafion content = 0.4), anode (Pt-Ru/C, 0.5 mg_{Pt} cm^{-2}), and cathode (Pt/C, 0.7 mg_{Pt} cm^{-2}). Commercial PA-PBI MEA component: PA-PBI membrane (50 μm thickness), PTFE binder, anode (Pt/C, 1.0 mg_{Pt} cm^{-2}), and cathode (Pt-alloy, 0.75 mg_{Pt} cm^{-2}). **(B)** *i*-*V* curve and power density of Nafion LT-PEMFC and AEMFC at 80 °C and 148 kPa (abs) backpressure under fully hydrated conditions. LT-PEMFC MEA component: commercial Gore MEA with reinforced PFSA membrane (15 μm thickness), Nafion ionomer, anode (Pt/C, 0.1 mg_{Pt} cm^{-2}), and cathode (Pt/C, 0.4 mg_{Pt} cm^{-2}). AEMFC MEA component: quaternized poly(phenylene) membrane (30 μm thickness), quaternized poly(fluorene) ionomer, anode (PtRu/C, 0.5 mg_{Pt} cm^{-2}), and cathode (Pt/C, 0.6 mg_{Pt} cm^{-2}). **(C)** Comparison of rated power density for different fuel cell technologies, sample code: fuel cell type (institution, cathode catalyst loading); LT-PEMFC (LANL, Pt/C, 0.1 mg_{Pt} cm^{-2}), LT-PEMFC (TU, Pt/N-KB, 0.105 mg_{Pt} cm^{-2}) [25], LT-PEMFC (GM, PtCo/C, 0.1 mg_{Pt} cm^{-2})[36], LT-PEMFC (NREL, PtCo/HSC, 0.078 mg_{Pt} cm^{-2})[26], AEMFC (LANL, Pt/C, 0.6 mg_{Pt} cm^{-2})[28], AEMFC (RPI, low loading Pt anode)[29], AEMFC (UD, Ag, 1 mg_{Ag} cm^{-2})[30], HT-PEMFC (RPI, Pt/C, 1 mg_{Pt} cm^{-2})[31], HT-PEMFC (Tianjin, 0.6 mg_{Pt} cm^{-2})[32], HT-PEMFC (DPS, 0.6 mg_{Pt} cm^{-2})[19], HT-PEMFC (KIST, 1 mg_{Pt} cm^{-2})[33], HT-PEMFC (LANL, 1 mg_{Pt} cm^{-2})[17], This study (LANL, 0.6 mg_{Pt} cm^{-2}).

Durability of the ion-pair HT-PEMFC with the protonated phosphonic acid electrodes

We evaluated the durability of the ion-pair HT-PEMFC under three operating conditions; (1) constant current density mode at 80 °C; (2) constant voltage mode at 160 °C; and (3) thermal cycling of 40 – 160 °C at 0.5 V. The durability of HT-PEMFCs at 80 °C is critical to the rapid start-up for automotive applications. The performance of the ion-pair HT-PEMFC at 80 °C and 0% inlet RH was reasonably high (PPD of 0.35 W cm^{-2} and HFR of ~0.15 Ω cm^2) (**Fig. S13**). The low-temperature durability of the ion-pair HT-PEMFC was evaluated at a constant current density of 0.2 A cm^{-2} and under high H_2/air stoichiometry of 72/30. In such high stoichiometry reactant flows, degradation of HT-PEMFCs is accelerated[19]. Under these conditions, no cell voltage loss or HFR decay for the ion-pair HT-PEMFC was measured during the 200 hours of operation (**Fig. 4A**). In contrast, the commercial PA-PBI HT-PEMFC exhibited a rapid cell voltage decay (10 mV h^{-1}) accompanied by an HFR increase and the cell stopped working after 40 hours of operation. The HFR gain of the PA-PBI HT-PEMFC during the durability test suggests a continuous loss of phosphoric acid over time.

The durability of the ion-pair HT-PEMFC was also evaluated at 160 °C under a high current density of 0.6 A cm^{-2} and H_2/air stoichiometry of 24/10 (**Fig. 4B**). The current density of the ion-pair HT-PEMFC gradually increased from 0.52 to 0.59 V during the first 1,000 hours, suggesting an electrode break-in process with phosphoric acid redistribution[23,24]. The voltage decay rate of the ion-pair HT-PEMFC after the first 1,000 hours was 3.3 μV h^{-1} and the HFR increase rate of the cell was 4.7 μΩ cm^2 h^{-1}. The stable performance of the ion-pair HT-PEMFC is also shown in the polarization curves during the life test (**Fig. S14**). Under similar high stoichiometry accelerate stress test (AST) conditions, the voltage decay rate of the commercial PA-PBI HT-PEMFC was 257 μV h^{-1} [23]. Considering that the voltage decay rate of a typical PA-PBI HT-PEMFC and LT-PEMFC under their optimized operating conditions (0.67 μV h^{-1} for PA-PBI[11] and 30–54 μV h^{-1} for LT-PEMFC[34,35]), the durability of the ion-pair HT-PEMFC under the AST conditions was excellent.

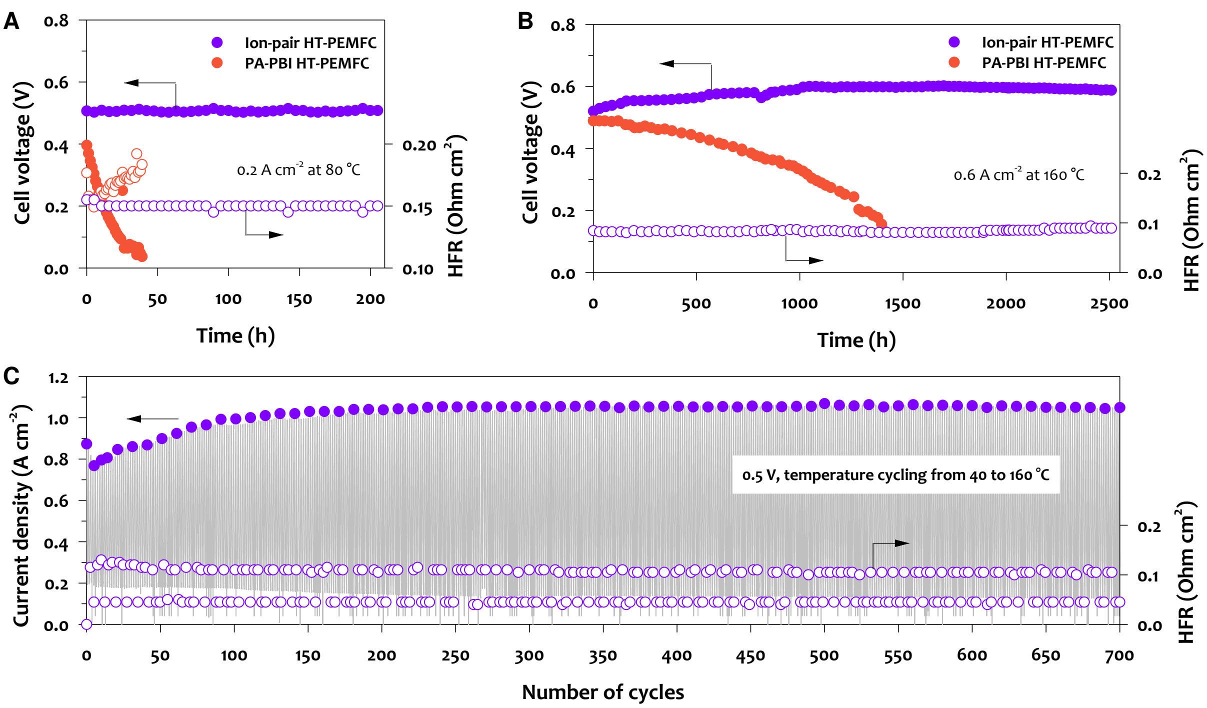

Figure 4 | Durability of ion-pair HT-PEMFC under H_2/air conditions. (A) Low-temperature durability test for the ion-pair and commercial PA-PBI HT-PEMFCs. Continuous measurement of cell voltage and HFR at a constant cell current density of 0.2 A cm^{-2} under anhydrous conditions, 148 kPa of applied backpressure and high stoichiometry of H_2/air (72/30) conditions. **(B)** High-temperature durability test for the ion-pair HT-PEMFC. Continuous measurement of cell voltage and HFR at a constant cell current density of 0.6 A cm^{-2} under anhydrous, 148 kPa of applied backpressure, and high stoichiometry H_2/air (24/10) conditions. For the life test at 160 °C, the cell was unintentionally stopped a few times including a major one due to hydrogen outage at ~800 hours. Ion-pair MEA: membrane: QAPOH-PA (40 µm thickness), ionomer: Nafion/PWN-1.8 (Nafion content = 0.5), anode (Pt-Ru/C, 0.5 mg_{Pt} cm^{-2}), cathode (Pt/C, 0.6 mg_{Pt} cm^{-2}). PA-PBI data was taken from literature[23]: cell temperature: 160 °C, H_2/air stoichiometry: 11.8/14.5 constant current density of 0.6 A cm^{-2} under anhydrous conditions. **(C)** Temperature cycling (40 – 160 °C) test for the ion-pair HT-PEMFC. Continuous measurement of cell current density and HFR (open symbols) at a constant cell voltage of 0.5 V under anhydrous conditions. The HFR values were measured at 40 °C (high number) and at 160 °C (low number).

We further evaluated the durability of the ion-pair HT-PEMFC using a thermal cycling AST protocol (**Fig. S15A**) to investigate the impact of thermal stress during the fuel cell startup-stop stage[36] as well as the impact of the dynamic current generation[37] (**Fig. 4C**). During the first 310 cycles, the cell current density at 40 °C slightly decreased from 0.18 to 0.14 A cm^{-2} while the current density at 160 °C increased from 0.77 to 1.05 A cm^{-2}. This behavior is probably due to the break-in process where the catalytic activity was enhanced during initial fuel cell operation. After 310 thermal cycles, the cell stabilized until the test was finished. The current density decay rate during the 310 – 700 thermal cycles calculated from the average value of the ten consecutive current density was 9.7 µA cm^{-2} cycle^{-1}. The corresponding current density decay after 10,000 startup-stop cycles was < 100 mA cm^{-2}. No notable HFR change was observed after the first 310 thermal cycles. For comparison, a commercial PA-PBI HT-PEMFC was subjected to the same AST and showed rapidly degrading behavior during the first 7 cycles and the cell became inoperable (**Fig. S15B**), confirming that the PA-PBI HT-PEMFC is difficult to run with frequent start up-stop cycles under load. Titration results revealed that the PA-PBI membrane lost 58% of initial phosphoric acid after 7 cycles, while the ion-pair membrane only exhibited a negligible 7% phosphoric acid loss after 700 cycles, reaffirming the superior phosphoric acid retention properties of the ion-pair HT-PEMFCs.

The demonstration of excellent performance and durability for the ion-pair HT-PEMFC presents opportunities in HDV fuel cell applications that require high device power and robustness. Our material platform enables ion-pair HT-PEMFCs which operate not only with the same overall thermal balance of the internal combustion engine but also generates substantially higher rated power than state-of-the-art LT-PEMFC making it well-suited for the automotive fuel cell applications.

Methods

Materials. The PA-PBI membrane/PTFE-bonded electrode MEAs (Celtec® P1100) produced through the polyphosphoric acid process were supplied by BASF Fuel Cells Inc. (Somerset, NJ, USA). The notation for these commercial MEAs are PA-PBI throughout the manuscript. Catalyst information of the MEA is as follows: anode catalyst: Pt/C (Pt loading: 1.0 mg_{Pt} cm^{-2}); cathode catalyst: Pt-alloy/C (Pt loading: 0.75 mg_{Pt} cm^{-2})[36]. PA-PBI PEM thickness was 50 μm.

For LT-PEMFCs, Nafion® membranes (Nafion® NR-211, 25.4 μm thickness) and Nafion D2020 dispersions were purchased from Ion Power, Inc. (New Castle, DE, USA). TEC10E40E: Pt 35.5% on high surface area carbon (Tanaka, TEC10E40E) were used for the anode and cathode (0.1 mg_{Pt} cm^{-2}). Carbon paper gas diffusion layers (SGL 29BC, GDLs) were used. We also used Gore MEA for comparison. For the fabrication of ion-pair MEAs, commercial 60% Pt/C (HiSPEC™ 9100) and 75% Pt-Ru/C (Pt:Ru = 2:1, HiSPEC™ 12100) were purchased from Alfa Aesar and Johnson Matthey, respectively. The Pt loading on the anode was 0.5 mg_{Pt} cm^{-2}. The Pt loadings on the cathode ranged from 0.1 – 0.7 mg_{Pt} cm^{-2}. For the ORR catalyst type study, we also used Tanaka Pt/C catalysts. TEC10E40E: Pt 35.5% on high surface area carbon, TEC10E20E: Pt 19.4% on high surface area carbon. GDLs for HT-PEMFC electrodes were CeTech W1S1009.

Preparation of QAPOH-PA ion-pair membranes. The QAPOH membranes were synthesized by an irreversible Diels–Alder reaction between bis(cyclopentadienone) and 1,4-diethynylbenzene[38,39]. This procedure produced a high molecular weight polymer (*Mw* = 450 kDA, polydispersity index = 5.3). This polymer was then acylated by attaching bromohexanoyl groups onto the poly(phenylene) backbone. The ketone group was removed by chemical reduction using triethylsilane and trifluoroacetic acid. The resultant functionalized polymer was then cast into films from chloroform. These films were then soaked in a 5 M solution of aqueous trimethyl amine to generate the QAPOH membranes. The QAPOH membranes were then soaked in a 1 M NaOH bath at room temperature overnight and subsequently washed thoroughly for over one hour with deionized water. After blotting excess water away, the nominally dry hydroxide form of the QAPOH membranes was soaked in an 85 wt% aqueous solution of phosphoric acid for 50 hours at room temperature. All phosphoric acid-doped QAPOH were used after removing the excess phosphoric acid on the membrane surface by blot drying.

Synthesis of phosphonated polymer (PWN). PWN was synthesized following a literature report[40]. Briefly explained here for PWN-1.8, poly(pentafluorostyrene), PFS (100 g, 515 mmol monomer units) was dispersed in dimethylacetamide, DMAc, (400 ml) and tris(trimethylsilsyl)phosphite, TMSP (200 g, 670 mmol) was added slowly. The reaction solution was then heated to 160 °C, and magnetically stirred overnight. After the reaction was completed, the warm mixture was precipitated in 2 L water and collected via filtration. The resulting white powder was refluxed in water three times for 30 min each, changing water each time, followed by boiling in a 2 wt% phosphoric acid solution. Washing with water until neutral and drying at 140 °C yielded the phosphonated polymer with 66% degree of phosphonation, PWN-1.8 (yield: 99%). The degree of phosphonation was controlled by the amount of tris(trimethylsilyl) phosphite phosphonating agent. The chemical structure of PWNs was characterized by an integral ratio between the resonances corresponding to the phosphonated (-134 ppm) and the non-phosphonated (-163 ppm) pentafluorophenyl rings of PWNs in the ^{19}F NMR. The IEC of PWNs obtained from the titration ranged from 0.9 to 3.0 mequiv. g^{-1}. The molecular weight of PWN was measured by a gel permeation chromatography (GPC eluent: water, standard: PSSNa, detector: Shodex RI 101). The number and weight average molecular weight of PWN-1.8 was 97 kDa and 136 kDa, respectively. The thermal decomposition temperature of the PWN, at which the first carbon monoxide evolvement in the Fourier transform infrared spectroscopy spectrum was observed, is 347 °C. Minimal degradation occurred over 100 hours at 200 °C. Absence of any ammonium group in the polymer side chain and phenyl group in the polymer backbone minimized the risk of catalyst poisoning[41,42].

Spectroscopy. The proton nuclear magnetic resonance (^1H NMR) spectra were recorded using a Bruker Avance 500 spectrometer (500 MHz) in deuterated dimethylsulfoxide (DMSO-d_6). Chemical shifts of the ^1H NMR spectra were referenced to tetramethylsilane (TMS) at 0 ppm as an internal reference.

^1H-NMR (400 MHz, DMSO-d_6, ppm) δ=8.36 (s, H), 4.33 (s, H), 3.77 (m, H), 2.94 (s, H), 2.78 (s, H), 1.95 (s, H), 1.02 (s, H) ^{19}F-NMR (250 MHz, DMSO-d_6, ppm) δ= -133.43 (bp 2F), -142.76 (bp, 2F), ^{31}P-NMR (101.2 MHz, DMSO-d_6, ppm) δ=-1.09 (bp,1P).

^{31}P NMR study. The samples of Nafion/PWN mixture for ^{31}P NMR spectra as a function of Nafion content were prepared inside the glove box using anhydrous DMSO-d_6 to avoid water contamination. A solution of 4 wt% PWN-1.8 in DMSO-d_6 was mixed with a different ratio of the proton form Nafion 212 solution in DMSO-d_6 in a vial, stirred at 60 °C for one hour and transferred into an NMR tube for the analysis.

Titration. The IEC of PWNs were determined by acid-base titration through the following procedures. All samples were dried at 100 °C for 12 hours before titration to obtain dry mass. The sample (H^+ form) was immersed to 1.0 M NaCl solution and stirred at room temperature for 24 hours, and the solution was titrated with 0.5 M NaOH solution using 2-3 drops of methyl orange aqueous solution (0.1%) as the indicator. IEC was calculated from the dry mass and the amount of NaOH used in titration.

The phosphoric acid-doping level of PEMs was determined by acid-base titration through the following procedure: i) PEM samples measuring 0.5 in. × 2 in. were weighed; ii) the PEM samples were titrated with 0.1 M NaOH solution using phenolphthalein as an indicator; iii) the samples were washed with water and dried in a vacuum plate at 100 °C for 3 hours and weighed again. The number of phosphoric acid per repeat unit (X) was calculated from the following equation:

$$X = \frac{V_{NaOH} \cdot C_{NaOH}}{\left(Eqiv_{mol} \times \left(\frac{W_{dry}}{M_W}\right)\right)} \quad (1)$$

where V_{NaOH} (l): the volume of NaOH

C_{NaOH} (mol/l): the molar concentration of NaOH

$Equiv_{mol}$: equivalent mole of titrant for PA which is 3; three moles of NaOH reacts with one more of phosphoric acid to produce trisodium phosphate.

W_{dry} (g): dry polymer weight

M_W (g/mol): the molecular weight of the polymer repeat unit.

The number of phosphoric acid per QA (or benzimidazole), (nPA_{QA}) was calculated from the following equation:

$$nPA_{QA} = \frac{(X \cdot 1000)}{(IEC \cdot M_W)} \quad (2)$$

where IEC (meq./g): ion exchange capacity of un-doped quaternized polymers.

DFT calculations. The pK_a value of pentafluorophenylphosphonic acid was calculated from a linear regression fit to deprotonation energies

$$pK_a = a(E_A^- - E_{HA}) + b \quad (3)$$

where E_A^- is the DFT calculated electronic energy of deprotonated acid and E_{HA} is the DFT calculated energy of the protonated acid[22]. As explained in our previous work, we derived a and b values using a data set of 9 experimental pK_a values. For each of these acids, we performed a full geometry optimization of both HA and the anion A^- using a SMD solvation model[43] with water as solvent at the M062X/6-311++G(d,p)[44] level using Gaussian09 program revision C.01[21]. Linear fitting of the data in Figure S1 results in the equation of line

$$pK_a = 0.108 * (E_A^- - E_{HA}) - 28.2 \quad (4)$$

with R2 of 0.90 and rms error of 0.2 pK_a units. $\Delta E = (E_A^- - E_{HA})$ for pentafluorophenyl phosphonic acid was calculated as 273.34 kcal/mol resulting in pK_a=1.3 $\pm$ 0.2.

$\Delta E = (E_A^- - E_{HA})$ for protonated pentafluorophenyl phosphonic acid was calculated as 257.92 kcal/mol resulting in pK_a=$-$0.4 $\pm$ 0.2.

^{31}P NMR chemical shifts were calculated using a gauge-including-atomic-orbital (GIAO) method as implemented in Gaussian09 program revision C.01[45]. In this case, the M062X/6-311+G(2d,p) level of theory was used. The geometries of the pentafluorophenyl phosphonic acid and the pentafluorophenyl phosphonic acid in coordination with the increasing number of Nafion fragments were first optimized after which the ^{31}P NMR chemical shifts were calculated.

The change in the Gibbs free energy for the formation of the anhydride was calculated using the MP2/6-31G(d) level theory as implemented in Gaussian09 quantum chemistry program revision C.01[22,40-43]. In all of the cases, the structure of acids and anhydrides were optimized and the change in the Gibbs free energy was calculated by performing the frequency analysis at 160 °C.

Thermogravimetric analysis. Thermal oxidative stability of the phosphonated polymer (PWN-1.8) was measured by TGA-FTIR (STA 449 F3 Jupiter ASC with Perseus-Coupling System from Netzsch). The temperature scan was performed from 30 to 600 °C at a heating rate of 5 °C min^{-1} in synthetic air (O_2: 70% and N_2: 30%).

Proton conductivity. The solution ionic conductivity[48] of the PWN and Nafion/PWN composite ionomers were measured using a custom liquid cell with 1 cm diameter stainless steel electrode area that was distanced apart by 1 cm and encased in polypropylene casing. A Nafion solution was prepared by the direct dissolution method using the proton form Nafion 212 (Nafion water content: 6 wt%)[46]. All samples were prepared at 2.5 or 5 wt% concentrations in anhydrous DMSO or NMP to mitigate solvent effects. The solution conductivity was measured using an AC impedance spectroscopy (Solartron 1260 gain phase analyser) over a frequency range from 1 Hz to 1 MHz.

For the in-plane film conductivity measurement for PWN and Nafion/PWN composite membranes, we prepared the membranes by solution casting. First, PWN polymers were dissolved in DMSO at 5 wt% with the acid of sonication at 40 °C. For the composite membrane, a commercial Nafion dispersion (D520, 5 wt%) was added at a desired blend ratio. The composite solution was clear under mild shaking or brief sonication. The composite solution was poured onto a glass petri dish. The petri dish was covered with a larger petri dish and a vial filled with methanol was placed on a hot plate at 80 °C inside a well-ventilated fume hood. After slow evaporation of the solvent overnight, it was placed in a petri dish with the membrane in a vacuum oven at 80 °C overnight to evaporate the residual solvent completely (**Fig. S7**). On the other hand, PWN solution was directly poured onto a petri dish and dried at 80 °C overnight in a convection oven. After cooling to room temperature, we detached the membrane from the glass substrate in deionized water. The membranes were stored in water. For the conductivity measurement of the membrane, we used a small window cell (width of the window: 0.5 cm). Before conductivity measurements, membranes samples were immersed in 85% phosphoric acid for at least 90 min. The membrane was placed between two platinum-coated electrodes and clamped tight. The window cell was placed in a convection oven, and the oven temperature was slowly increased to 120 °C for 30 minutes. The membrane's impedance was measured using an AC impedance spectroscopy (Solartron 1260 gain phase analyzer). The temperature was then increased to 240 °C, and the conductivity was measured at every 20 °C interval until the temperature reached 80 °C.

HAADF-STEM images and corresponding EDS elemental maps (Pt+F+C). Samples for the transmission electron microscopy (TEM) analysis were prepared by microtoming epoxy-embedded small sections (1 cm× 0.5 cm) of the electrodes. Epoxy was prepared using a 1:1 (weight) mixture of trimethylolpropane triglycidyl ether resin (Sigma-Aldrich, USA) and 4,4′-Methylenebis (2-methylcyclohexylamine, Sigma-Aldrich, USA) hardener, and embedded sections were polymerized overnight at 60 °C. The thin (~100 nm) electrode cross-sections were placed on 200 mesh Cu/Pd grids. A Talos 200kV transmission electron microscope

(Thermo Fisher Scientific, USA) with four Super-X silicon drift detectors for energy dispersive spectrometry (EDS) was used for the TEM and a high-angle annular dark-field scanning transmission electron microscopy (HAADF-STEM) imaging and EDS elemental mapping were used as well. The EDS mapping was performed at 5k× and 79k× magnifications, with a 1000 µs dwell time for 1 cycle, and electron dose of 2.34x104 e^{-}/nm^2. The maps processing, elemental analysis and visualization was completed using ESPIRIT 1.9 (Bruker, USA) analytical software.

MEA fabrication. MEAs were fabricated from catalyst inks containing Pt/C catalysts or Pt-Ru/C catalysts and single ionomer or composite ionomer dispersions (the solid content = 5 wt%). For the PWN ionomer dispersion, we used NMP. For the Nafion dispersion, we used a water/isopropanol mixture (water content: 15 wt%). For the anode of the ion-pair HT-PEMFC, a Pt-Ru/C catalyst (Pt:Ru 2:1, HiSPEC 12100) was used to minimize the adverse phenyl adsorption from the ionomer[42]. The composite ionomer dispersions were prepared by mixing the PWN and Nafion ionomer dispersions with a different ratio to obtain the Nafion content of 0, 0.3, 0.4, 0.5, 0.6 and 1.0. The catalyst ink was sonicated in an ultrasonic bath for an hour to make a uniform dispersion and painted on the GDLs (W1S1009, CeTech) by hand painting until the Pt loadings reached 0.5 mg cm^{-2} and 0.7 mg cm^{-2} for anode and cathode, respectively. Once the hand painting was finished, the gas diffusion electrodes (GDEs) were left on the vacuum plate for 10 min at 70 °C to remove the residual dispersion agent within the electrodes. The catalyst coated GDEs were sandwiched with a QAPOH-PA PEM (35 µm thick). The active area of each MEA was 5 cm^2. For control, a Nafion-based LT-PEMFC MEA, Nafion 211 membrane and Nafion D2020 (20 wt%) ionomer were purchased from Ion Power. The ionomer to carbon (I/C) ratio by mass was 0.9. The Pt/C catalyst and D2020 ionomer were dispersed in a deionized H_2O and 1-propanol (4:3 volume ratio) mixture by stirring at 700 rpm for 4 hours, then under an ultrasonication bath for 20 minutes. For the cathode, the Pt/C catalyst was deposited on the membrane via ultrasonic spray coating. For the anode, TEC10V20E Pt/VC (Vulcan XC-72 carbon) was used for all experiments and was also spray-coated on the membrane after the cathode was spray coated. Pt loading was fixed to be around 0.1 mg_{Pt} cm^{-2} (±10%) for both the cathode and anode (confirmed by XRF). The active area of the catalyst-coated membrane was 5 cm^2. GDLs for HT-PEMFC electrodes were CeTech W1S1009 and for LT-PEMFC MEAs, SGL 29BC carbon paper GDLs were used throughout all MEA tests. Reinforced PTFE gaskets were used for ion-pair HT-PEMFCs. Polyurethane gaskets were used for Nafion-based LT-PEMFCs.

Fuel cell performance and durability. The fuel cell performance of the MEAs was measured using a fuel cell test station (Fuel Cell Technologies, Inc.). For HT-PEMFCs, polarization curves and the HFR of MEAs were obtained at temperatures ranging from 80 to 200°C. H_2 and air (pressure was set at 10 psig corresponding backpressure of 148 $kPa_{absolute}$) were supplied at a rate of 500 and 500 sccm, respectively, or otherwise noted within the manuscript. The cell current density and HFR were measured every minute without external humidification. For the test of Nafion-based LT-PEMFC control MEA, polarization curves and the HFR of the MEAs were obtained at temperature ranging from 80 to 100 °C. H_2 and air (backpressure set at 148 kPa) were supplied at a rate of 500 and 500 sccm, respectively. After we found the best-performing ionomer and its composition, we further optimized the electrode formulation and reactant stoichiometry. Negligible change in the MEA performance was observed, reducing the cathode Pt loading to 0.3 mg_{Pt} cm^{-2} from 0.6 mg_{Pt} cm^{-2}. Note that the MEA with 60 wt% Pt metal content catalyst (Johnson Matthey, HiSPEC™ 9100) performed better than the MEAs with lower Pt metal content catalysts (Tanaka Precious Metals, TEC10E40E and TEC10E20E), suggesting that highly active Pt/C catalysts for LT-PEMFCs may not work well for HT-PEMFCs, as the reaction environment of HT-PEMFCs is different.

The stability of ion-pair HT-PEMFCs was evaluated. Steady state H_2/air durability tests were performed at 80 and 160 °C. For 80 °C conditions, cell voltage and HFR were measured for 200 hours under constant current density of 0.2 A cm^{-2}. The corresponding H_2/air stoichiometry was 72/30. The backpressure was 148 kPa. For 160 °C conditions, cell voltage and HFR were measured for 2,000 hours under constant current density of 0.6 A cm^{-2}. High gas flow was used (500 sccm/500 sccm for H_2/air) to accelerate fuel cell degradation[20]. The corresponding H_2/air stoichiometry was 24/10. The backpressure was 148 kPa.

Two temperature cycling H_2/air durability tests were performed. For the first temperature cycling AST, a temperature cycling protocol consisting of triangular thermal cycles from 80 to 160 °C with a ramp of 10 °C min^{-1} was performed at a constant current density of 0.15 A cm^{-2}. The anode and cathode inlet dew point was fixed to 40 °C and backpressure was set at 148 kPa (absolute). The cell's HFR was measured each time the cell temperature reached 80 or 160 °C. The second thermal cycling AST consisted of deep triangle thermal cycles from 40 to 160 °C with a ramp of 15 °C min^{-1} under anhydrous conditions to simulate cold start-up cycles. A constant voltage of 0.5 V was applied and the current density monitored as a function of time. The HFR was measured when the cell temperature reached either 40 or 160 °C.

Rated power calculation. The heat rejection requirement has been expressed as a constraint that a nominal 90-kW$_e$ fuel cell stack should have waste heat (Q)/ΔT less than 1.45 kW °C^{-1}, where ΔT is the initial temperature difference between the stack coolant outlet temperature (T_c) and the ambient temperature (T_a) and Q is defined as [stack power (90-kW$_e$) × (1.25 V – voltage at rated power)/(voltage at rated power)][6]. The rated power was calculated to meet the (Q)/ ΔT = 1.45 kW °C^{-1} target at the cell voltage, i.e., 77.6 / ((22.1 + $T[°C]$)).

Electrochemical impedance spectroscopy. Electrochemical impedance spectroscopy (EIS) of the HT-PEMFC was evaluated by Biologic SP-200 after measuring the polarization curve and HFR. The spectra were recorded by sweeping frequencies over the range 1 MHz – 0.1 Hz at a dc voltage of 0.8 and 0.6 V and constant current density of 1.2 A cm^{-2}. The experimental spectra were fitted to equivalent circuits by employing EC-Lab software. The equivalent circuit applied here consists of ohmic resistance (R_{ohm}) in series with two parallel constant phase elements, CPE_{ct}/R_{ct} for charge transfer resistance and CPE_{mt}/R_{mt} for the mass transport resistance[47,48].

References

1. Cano, Z.P. et al. Batteries and Fuel Cells for Emerging Electric Vehicle Markets. *Nat. Energy* **3**, 279-289 (2018).

2. Cullen, D. A. et al. New roads and challenges for fuel cells in heavy-duty transportation. *Nat. Energy* https://doi.org/10.1038/s41560-021-00775-z (2021).

3. Forrest, K., Kinnon, M. M., Tarroja, B. & Samuelsen, S. Estimating the technical feasibility of fuel cell and battery electric vehicles for the medium and heavy duty sectors in California. *Appl. Energy* **276**, 115439 (2020).

4. Hong, B. K., Kim, S. H. & Kim, C. M. Powering the future through hydrogen and polymer electrolyte membrane fuel cells current commercialisation and key challenges with focus on work at Hyundai. *Johnson Matthey Technol. Rev.* **64**, 236-251 (2020).

5. Gittleman, C. S., Jia, H., De Castro, E. S., Chisholm, C. & Kim, Y. S. Proton conductors for heavy-duty vehicle fuel cells. *Joule* submitted (2021).

6. U. S. Department of Energy *Fuel Cell Technical Team Roadmap* (U. S. Drive Partnership, 2017);https://www.energy.gov/sites/prod/files/2017/11/f46/FCTT_Roadmap_Nov_2012_FINAL.pdf

7. Valdés-López, V. F., Mason, T., Shearing, P. R. & Brett, D. J. L. Carbon monoxide poisoning and mitigation strategies for polymer electrolyte membrane fuel cells - A review. *Prog. Energy Combust. Sci.* **79**, 100942 (2020).

8. Dicks, A. L. & Rand, D. A. J. *Proton-Exchange Membrane Fuel Cells in Fuel Cell Systems Explained* pp. 69-133 (John Wiley & Sons Ltd, ed. 3, 2018).

9. Park, C. H. et al. Nanocrack-regulated self-humidifying membranes. *Nature* **532**, 480-483 (2016).

10. Yang, J. S. et al. High molecular weight polybenzimidazole membranes for high temperature PEMFC. *Fuel Cells* **14**, 7-15 (2014).

11. Pingitore, A. T., Huang, F., Qian, G. Q. & Benicewicz, B. C. Durable high polymer content m/p-polybenzimidazole membranes for extended lifetime electrochemical devices. *ACS Appl. Energy Mater.* **2**, 1720-1726 (2019).

12. Jakobsen, M. T. D. *High temperature polymer electrolyte membrane fuel cells: Approaches, Status, and Perspectives*, Li, Q., Aili, D., Hjuler, H. A. & Jensen, J. O. eds. (Springer International Publishing, 2016).

13. Lee, K. S., Spendelow, J. S., Choe, Y. K., Fujimoto, C. & Kim, Y. S. An Operationally flexible fuel cell based on quaternary ammonium-biphosphate ion pairs. *Nat. Energy* **1**, 16120 (2016).

14. Lee, A. S., Choe, Y. K., Matanovic, I. & Kim, Y. S. The energetics of phosphoric acid interactions reveals a new acid loss mechanism. *J. Mater. Chem. A* **7**, 9867-9876 (2019).

15. Rager, T., Schuster, M., Steininger, H. & Kreuer, K. D. Poly(1,3-phenylene-5-phosphonic acid), a fully aromatic polyelectrolyte with high ion exchange capacity. *Adv. Mater.* **19**, 3317-3321 (2007).

16. Parvole, J. & Jannasch, P. Polysulfones grafted with poly(vinylphosphonic acid) for highly proton conducting fuel cell membranes in the hydrated and nominally dry state. *Macromolecules* **41**, 3893-3903 (2008).

17. Atanasov, V. et al. Synergistically Integrated Phosphonated Poly(pentafluorostyrene)s for Fuel Cells. *Nat. Mater.* **20**, 370-377 (2021).

18. Kongkanand, A. & Mathias, M. F. The priority and challenge of high-power performance of low-platinum proton-exchange membrane fuel cells. *J. Phys. Chem. Lett.* **7**, 1127-1137 (2016).

19. Søndergaard, T. et al. Long-term durability of PBI-based HT-PEM fuel cells: effect of operating parameters. *J. Electrochem. Soc.* **165**, F3053-F3062 (2018).

20. Haouas, M., Taulelle, F., Prudhomme, N. & Cambon, O. NMR analysis of $GaPO_4$ crystal growth in mixtures of phosphoric and sulfuric acids. *J. Cryst. Growth* **296**, 197-206 (2006).

21. Frisch, M. J. et al. *Gaussian 09 Revision C.01* (Gaussian, Inc., 2010).

22. Zhang, S. M., Baker, J. & Pulay, P. A reliable and efficient first principles-based method for predicting pK(a) values. 1. Methodology. *J. Phys. Chem. A* **114**, 425-431 (2010).

23. Eberhardt, S. H. et al. Dynamic operation of HT-PEFC: In-operando imaging of phosphoric acid profiles and (re)distribution. *J. Electrochem. Soc.* **162**, F310-F316 (2015).

24. Lee, K. -S. et al. Intermediate temperature fuel cells via an ion-pair coordinated polymer electrolyte. *Energy Environ. Sci.* **11**, 979-987 (2018).

25. Maurya, S. et al. Rational design of polyaromatic ionomers for alkaline membrane fuel cells with > 1 W cm^{-2} power density. *Energy Environ. Sci.* **11**, 3283-3291 (2018).

26. Ott, S. et al. Ionomer distribution control in porous carbon-supported catalyst layers for high-power and low Pt-loaded proton exchange membrane fuel cells. *Nat. Energy* **19**, 77-85 (2020).

27. Cleve, T. V. et al. Tailoring electrode microstructure via ink content to enable improved rated power performance for platinum cobalt/high surface area carbon based polymer electrolyte fuel cells. *J. Power Sources* **482**, 228889 (2021).

28. Lai, Y. -H. et al. Accelerated stress testing of fuel cell membranes subjected to combined mechanical/chemical stressors and cerium migration. *J. Electrochem. Soc.* **165**, F3100-F3103 (2018).

29. Noh, S., Jeon, J. Y., Adhikari, S., Kim, Y. S. & Bae, C. Molecular engineering of hydroxide conducting polymers for anion exchange membranes in electrochemical energy conversion technology. *Acc. Chem. Res.* **52**, 2745-2755 (2019).

30. Wang, J. et al. Poly(aryl piperidinium) membranes and ionomers for hydroxide exchange membrane fuel cells. *Nat. Energy* **4**, 392-398 (2019).

31. Mader, J., Xiao, L., Schmidt, T. J. & Benicewicz, B. C. Polybenzimidazole/acid complexes as high-temperature membranes. *Adv. Polym. Sci.* **216**, 63-124 (2008).

32. Li, X. et al. Highly conductive and mechanically stable imidazole-rich cross-linked networks for high-temperature proton exchange membrane fuel cells. *Chem. Mater.* **32**, 1182-1191 (2020).

33. Krishnan, N. N. et al. Phosphoric acid doped crosslinked polybenzimidazole (PBI-OO) blend membranes for high temperature polymer electrolyte fuel cells. *J. Membr. Sci.* **544**, 416-424 (2017).

34. Xie, J., Wood, D. L., More, K. L., Atanassov, P. & Borup, R. L. Microstructural changes of membrane electrode assemblies during PEFC durability testing at high humidity conditions. *J. Electrochem. Soc.* **152**, A1011-A1020 (2005).

35. Yu, J. R., Matsuura, T., Yoshikawa, Y., Islam, M. N. & Hori, M. In situ analysis of performance degradation of a PEMFC under nonsaturated humidification. *Electrochem. Solid-State Lett.* **8**, A156-A158 (2005).

36. Schmidt, T. J. & Baurmeister, J. Properties of high-temperature PEFC Celtec (R)-P 1000 MEAs in start/stop operation mode. *J. Power Sources* **176**, 428-434 (2008).

37. Borup, R. et al. Scientific aspects of polymer electrolyte fuel cell durability and degradation. *Chem. Rev.* **107**, 3904-3951 (2007).

38. Hibbs, M. R. Alkaline stability of poly(phenylene)-based anion exchange membranes with various cations. *J. Polym. Sci. Part:B Polym. Phys.* **51**, 1736-1742 (2013).

39. Maurya, S., Fujimoto, C., Hibbs, M. R., Villarrubia, C. N. & Kim, Y. S. Toward improved alklaine membrane fuel cell performance using quaternized aryl-ether free polyaromatics. *Chem. Mater.* **30**, 2188-2192 (2018).

40. Atanasov, V. & Kerres, J. Highly phosphonated polypentafluorostyrene. *Macromolecules* **44**, 6416-6423 (2011).

41. Chung, H. T., Martinez, U., Chlistunoff, J., Matanovic, I. & Kim, Y. S. Cation-hydroxide-water co-adsorption inhibits the alkaline hydrogen oxidation reaction. *J. Phys. Chem. Lett.* **7**, 4464-4469 (2016).

42. Matanovic, I., Chung, H. T. & Kim, Y. S. Benzene adsorption: A significant inhibitor for the hydrogen oxidation reaction in alkaline conditions. *J. Phys. Chem. Lett.* **8**, 4918-4924 (2017).

43. Marenich, A. V., Cramer, C. J. & Truhlar, D. G. Universal solvation model based on solute electron density and on a continuum model of the solvent defined by the bulk dielectric constant and atomic surface tensions. *J. Phys. Chem. B* **113**, 6378-6396 (2009).

44. Zhao, Y. & Truhlar, D. G. The M06 suite of density functionals for main group thermochemistry, thermochemical kinetics, noncovalent interactions, excited states, and transition elements: two new functionals and systematic testing of four M06-class functionals and 12 other functionals. *Theor. Chem. Acc.* **120**, 215-241 (2008).

45. Gao, X. Q. et al. High performance anion exchange ionomer for anion exchange membrane fuel cells. *RSC Adv.* **7**, 19153-19161 (2017).

46. Kim, Y. S. et al. Origin of toughness in dispersion-cast Nafion membranes. *Macromolecules* **48**, 2161-2172 (2015).

47. Asghari, S., Mokmeli, A. & Samavati, M. Study of PEM fuel cell performance by electrochemical impedance spectroscopy. *Int. J. Hydrog. Energy* **35**, 9283-9290 (2010).

48. Stampino, P. G. et al. Investigation of hydrophobic treatments with perfluoropolyether derivatives of gas diffusion layers by electrochemical impedance spectroscopy in PEM-FC. *Solid State Ion.* **216**, 100-104 (2012).

Acknowledgements

PA-PBI samples were provided by Dr. E. S. De Castro (Advent Technologies). We thank A. Muenchinger (MPI), K. D. Kreuer (MPI) for the conductivity data on PWN. This work was supported by the U.S. Department of Energy, Energy Efficiency and Renewable Energy, Fuel Cell Technology Office (L'innovator program) and Advanced Research Projects Agency-Energy (Award number: DE-AR0001003). The synthesis of PWN polymer was developed and supported by the following German National Projects: DFG KE 673/10-1 Nr. 576968, BMBF 03SF0432B and 03SF0531C. A.S. Lee acknowledges support from the KIST internal research program and the National R&D Program through the National Research Foundation of Korea (NRF) funded by the Ministry of Science and ICT (2020M3H4A3106354, 2020M3H4A3106403). Los Alamos National Laboratory is operated by Triad National Security, LLC under US Department of Energy Contract Number 89233218CNA000001.

Sandia National Laboratories is a multi-mission laboratory managed and operated by National Technology and Engineering Solutions of Sandia, LLC, a wholly owned subsidiary of Honeywell International, Inc., for the U.S. Department of Energy's National Nuclear Security Administration under contract DE-NA0003525. I.M. thankfully acknowledges the computational resources from the Tri-Lab computing resources of LANL, NERSC, a DOE Office of Science User Facility supported by the Office of Science of the U.S. Department of Energy under contract no. DE-AC02-05CH11231, and CARC, UNM Center for Advanced Research Computing.

Author contributions

A.S.L. and Y.S.K. developed the intellectual concept and designed all the experiments of this research. V.A., J.K., S.A., and C.F. prepared the polymeric materials. E.J.P., S.M., L.D.M., J.J. and H.J. synthesized model compound and performed electrochemical experiments. J.J did TEM and image analysis. K.H.L. S.M. and A.S.L. performed fuel cell testing. I.M. performed the DFT calculations. K.H.L, A.S.L, and Y.S.K analyzed all experimental data and wrote the paper.

Additional information

Supplementary information is available for this paper. Reprints and permissions information is available at www.nature.com/reprints. Correspondence and requests for materials should be addressed to Y.S.K.

Competing interests

A.S.L and Y.S.K have filed a patent application no. 17/196283 on March 9, 2021 related to the ionomer composition described in this article.

Supplementary Files

This is a list of supplementary files associated with this preprint. Click to download.

- SupplementaryinformationNatureEnergy.docx